This article has been accepted for publication in a future issue of this journal, but has not been fully edited. Content may change prior to final publication. Citation information: DOI 10.1109/LWC.2021.3119221, IEEE Wireless Communications Letters

UAV Location Optimization in MISO ZF Pre-coded VLC Networks

Mahmoud Wafik Eltokhey, Mohammad-Ali Khalighi, Zabih Ghassemlooy

***Abstract*—Use of unmanned aerial vehicles (UAVs) to provide on-demand communications has been receiving growing interest, especially for use in remote and hard-to-reach areas. Also, the use of light-emitting diode -based lighting in UAVs has opened opportunities for data transmission through visible-light communications. To manage multi-user interference while avoiding complex handover procedures, we consider the use of zero forcing (ZF) pre-coding. Since the performance of ZF pre-coding depends on the correlation between channel gains of users, we propose in this paper to reduce it by means of location optimization of UAVs. More specifically, we use particle swarm optimization with the objective of maximizing the overall achievable network throughput. Furthermore, to relax the optimization requirements at UAVs, we investigate the case when the optimization is performed at a specific rate under different mobility conditions.**

***Index Terms*—Visible-light communications; unmanned-aerial vehicles; ZF pre-coding; particle swarm optimization.**

I. Introduction

Visible-light communication (VLC) systems exploit the light-emitting diode (LED)-based luminaires to provide simultaneous lighting and data communications [1]. The growing use of LEDs for illuminations in unmanned aerial vehicles (UAVs) (i.e., drones) has opened up opportunities for VLC applications such as surveillance and monitoring, data collection from Internet-of-things devices, off-loading traffic data from base stations (BSs), and improving quality-of-service for the users. Recently, the concept of Twinkle was proposed in [2], where LEDs mounted on UAVs were used for illumination in urban areas. In addition, UAVs with LED-based lights have been reported for operations at night time [3].

Use of UAVs as flying BSs to provide on-demand wireless communications offers a cost-effective and flexible solution in a number of applications [4]. Here, RF-based transmission may result in interference with the ground networks, and may also decrease the applicability of high-speed communications due to the limited energy [4]. VLC-based transmission is an interesting alternative, since it maximizes the resource utilization by using the existing LED-based lights. This combined feature of illumination and data communication is much favored in search and rescue, delivery by drone at night, path illumination by UAVs in areas with no lighting, etc. [3], as well as in large space indoor industrial scenarios. The use of VLC in UAV-based networks has received particular interest in the recent literature. For instance, optimizing UAV location and user association was considered in [3] to minimize UAV power consumption, which was further extended in [4] using deep learning. Also, [5] considered network sum-rate maximization for non-orthogonal multiple access UAV-based VLC networks, by optimizing the power allocation and UAVs' placement.

In [3]–[5], each user was associated with a single cell, which needs dealing with handover and cell-based inter-user interference. To avoid handovers while mitigating inter-user and inter-cell interferences [6], multiple-input multiple-output techniques can be used [7] but the constraints on the receiver (Rx) array size to ensure a full-rank channel matrix makes multiple-input single-output (MISO) technique a more suitable solution in practice [8]. In multi-user (MU) MISO VLC systems with single PD-based Rxs [8], [9], linear zero forcing (ZF) pre-coding is widely considered, as it offers simplicity and improved performance at high signal-to-noise ratios (SNRs) [10], [11]. However, the performance of linear ZF pre-coding is affected by the user locations, which impacts the correlation between the users' channel gains. In fact, a higher correlation in the network channel matrix results in a degraded ZF pre-coding performance, i.e., a lower network sum-rate. In this paper, we propose to decrease this correlation by optimizing the locations of UAVs using particle swarm optimization (PSO). Note that, PSO has been used in optical wireless communications, e.g., for optimizing the diffuse spot locations [12] and resource allocation [13]. Our main contributions include: (i) proposing the use of ZF pre-coding in UAV-based VLC networks, which to the best of our knowledge has not been addressed before; (ii) proposing to decrease the correlation in the network channel matrix by PSO-based UAV location optimization; and (iii) studying the effect of varying the optimization parameters on the network performance.

II. System Model and Mathematical Formulation

A. VLC System Model

Consider a UAV-based VLC system as in Fig. 1. Each UAV acts as an access point (AP), where the LED-based APs mounted on UAVs provide illumination and VLC downlink to the Rxs for data communication. A central control unit, which is mounted on one of the UAVs, or located in a separate central UAV (not used for direct communication with the Rxs), exchanges information with the APs and is, in turn,

M. W. Eltokhey and M. A. Khalighi are with Aix-Marseille University, CNRS, Centrale Marseille, Institut Fresnel, Marseille, France (e-mail: Mahmoud.Eltokhey@centrale-marseille.fr, Ali.Khalighi@fresnel.fr)

Z. Ghassemlooy is with Optical Communications Research Group, Faculty of Engineering and Environment, Northumbria University, Newcastle upon Tyne, NE1 8ST, UK (e-mail: z.ghassemlooy@northumbria.ac.uk)

This work has received funding from the European Union's Horizon 2020 research and innovation programme under the Marie Skłodowska-Curie grant agreement No. 764461 (VisIoN), and was based upon work from European Union's Horizon 2020 COST Action CA19111 (NEWFOCUS).

This article has been accepted for publication in a future issue of this journal, but has not been fully edited. Content may change prior to final publication. Citation information: DOI 10.1109/LWC.2021.3119221, IEEE Wireless Communications Letters

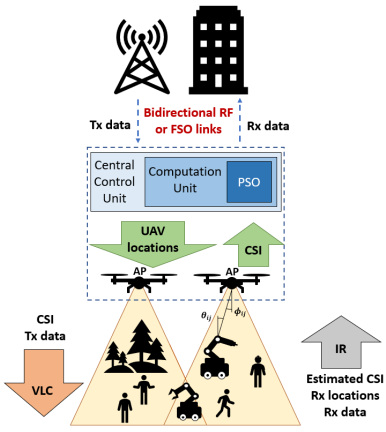

Fig. 1: Illustration of the considered system with the flow of information between a cellular network, a central control unit, UAV APs, and Rxs.

connected to a cellular network via an RF or a free-space optical link. Infrared uplinks are used for sending data and estimated channel-state information (CSI) to the APs; this latter being used in the central control unit for determining the ZF pre-coding matrix and for UAV location optimization.

Let us denote by h_{ij} the channel coefficient between the i^{th} AP and the j^{th} Rx. We account only for the line-of-sight (LOS) path in h_{ij}, given the heights of the APs and the dominance over the non-LOS paths. For complying with the constraints of ZF pre-coding, we consider that the number of Rxs (N_r) is less than or equal to the number of APs (N_t) [8]. The transmission by the considered LED luminaires can be modeled by Lambertian pattern of order m, where [1]:

$$h_{ij} = \rho_j \, \mathcal{S} \, \frac{(m+1)}{2\pi \, l_{ij}^2} \cos^m(\phi_{ij}) \cos(\theta_{ij}) A_{\text{PD}_j}. \tag{1}$$

Here, ϕ_{ij} and θ_{ij} refer to the angles of emission and incident with respect to AP_i and Rx_j, respectively, and l_{ij} denotes the related link distance. Also, ρ_j and A_{PD_j} are the responsivity and the surface area of the PD, respectively, and $\mathcal{S}$ is the LED conversion efficiency. Note, for θ_{ij} larger than the field-of-view (FOV) of Rx_j, we have $h_{ij} = 0$.

B. ZF Pre-coding

In the considered MU-MISO system, to eliminate MU interference, ZF pre-coding is applied to the signals of the Rxs. At the i^{th} AP, the transmit signal is [8]:

$$x_i = \sum_{j=1}^{N_r} w_{ij} \, d_j + I_{\text{DC}i}, \tag{2}$$

where d_j is the desired signal of the j^{th} Rx, w_{ij} is the pre-coding weight, and $I_{\text{DC}i}$ is the DC bias. At Rx_j, after removing the DC offset, the received signal is given by:

$$r_j = \sum_{i=1}^{N_t} x_i h_{ij} + z_j = \boldsymbol{h}_j^T \, \boldsymbol{w}_j^T \, d_j + \sum_{k \neq j} \boldsymbol{h}_j^T \, \boldsymbol{w}_k^T \, d_k + z_j, \tag{3}$$

where $\boldsymbol{h}_j = [h_{1,j}, ..., h_{N_t,j}]^T$ is the vector of the channel gains associated with Rx_j; $(\cdot)^T$ stands for transposition; $\boldsymbol{d} = [d_1, ..., d_{N_r}]$ is the vector of the desired signals; $\boldsymbol{w}_j = [w_{1,j}, ..., w_{N_t,j}]$ is the pre-coding vector associated with Rx_j; and z_j is Gaussian noise with variance σ_n^2, representing the ambient light induced shot noise and the thermal noise. The 1st and 2nd terms on the right hand side in (3) represent the desired signal and the interference, respectively. Let $\boldsymbol{r} = [r_1, ..., r_{N_r}]$ denote the vector of the received signals. We have:

$$\boldsymbol{r} = \boldsymbol{H} \, \boldsymbol{W} \, \boldsymbol{d} + \boldsymbol{z}, \tag{4}$$

where $\boldsymbol{H} = [\boldsymbol{h}_1^T, ..., \boldsymbol{h}_{N_r}^T]^T$, $\boldsymbol{W} = [\boldsymbol{w}_1^T, ..., \boldsymbol{w}_{N_r}^T]$, and $\boldsymbol{z} = [z_1, ..., z_{N_r}]$ denote the network channel matrix, the pre-coding weights matrix, and vector of noise component of all Rxs, respectively. For linear ZF pre-coding, $\boldsymbol{W}$ is given by [8]:

$$\boldsymbol{W} = \boldsymbol{H}^T \, (\boldsymbol{H} \, \boldsymbol{H}^T)^{-1} \, \text{diag}(\boldsymbol{\gamma}), \tag{5}$$

where $\boldsymbol{\gamma}$ denotes a diagonal matrix, composed of diagonal entries $\gamma_j > 0$, such that γ_j values can be regarded as the coefficients of parallel sub-channels determined based on a design criterion. For the sake of simplicity, we consider the criterion of maximizing the minimum achievable throughput. Defining $\boldsymbol{\mu} = [\mu_1, ..., \mu_{N_r}] = \left[\frac{\gamma_1}{\sigma_1}, ..., \frac{\gamma_{N_r}}{\sigma_{N_r}}\right]$, this gives [8]:

$$\boldsymbol{\mu} = \mu^* \mathbf{1}; \; \mu^* = \frac{\sqrt{P_e}}{\max(\boldsymbol{A} \, \mathbf{1})}, \tag{6}$$

where $\boldsymbol{A} = \text{abs}\big(\boldsymbol{H}^T (\boldsymbol{H} \boldsymbol{H}^T)^{-1}\big) \, \text{diag}(\boldsymbol{\sigma})$; $\boldsymbol{\sigma}$ is the Rxs' noise variance vector; abs(.) applies the absolute value operation for each element; $\mathbf{1}$ is a vector with all entries equal to one; and P_e is the transmit electrical power per AP. For Rx_j, the SNR and the maximum achievable throughput are given as, respectively:

$$\text{SNR}_j = \frac{\left(\boldsymbol{h}_j^T \, \boldsymbol{w}_j^T\right)^2}{\sigma_n^2} = \frac{\gamma_j^2}{\sigma_n^2}, \tag{7}$$

$$R_j = \frac{B}{2} \log_2 \left(1 + \text{SNR}_j\right) \quad \text{(bps)}, \tag{8}$$

where (8) assumes DC-biased optical-orthogonal frequency-division multiplexing with a penalty of factor 2 due to Hermitian symmetry, and B denotes the system bandwidth. Note that, the achievable data rate depends on the UAVs' locations by affecting the path loss, as well as the correlation in $\boldsymbol{H}$.

III. UAV Location Optimization

To optimize the UAV locations, we consider the well-established algorithm of PSO, which is a metaheuristic optimization technique that mimics the swarms movement [14]. Given the non-linear nature of the considered problem and the available degrees of freedom by change in the UAVs' locations, PSO is an efficient approach, which can converge to high quality solutions at low complexity. This is an important point, allowing real-time adaptivity to the mobility of the users, given the possible limitations on the computational resources.

A. Particle Swarm Optimization

In PSO, each point in the D-dimension search space represents a solution; particles travel between the points to find the optimal solution. For each particle's movements, both the speed and the directions are influenced by its best

experience (i.e., its best solution so far, P_{best}), and by the best position found by the ensemble of particles (i.e., the global best position, G_{best}). The quality of the solution is evaluated based on a fitness function. Assuming the number of iterations $N_{\max_{it}}$ and the number of particles $N_{\max_p}$, applied to an optimization problem with the number of variables D, for the particle q at iteration ℓ, the algorithm updates the vectors of particle's position $\boldsymbol{p}_q = [p_{q1}, p_{q2}, ..., p_{qD}]$; velocity $\boldsymbol{v}_q = [v_{q1}, v_{q2}, ..., v_{qD}]$; and personal best position $\boldsymbol{P}_{\text{best,q}} = [p_{\text{best},q1}, p_{\text{best},q2}, ..., p_{\text{best},qD}]$. In addition, if a q^{th} particle offers a superior fitness than that achieved by the position in the global best position vector $\boldsymbol{G}_{\text{best}} = [g_{\text{best},1}, g_{\text{best},2} ..., g_{\text{best},D}]$, $\boldsymbol{G}_{\text{best}}$ is updated by the position of the q^{th} particle. To update the velocity of particle q at iteration $\ell + 1$ for the variable d, the following equation is used [14]:

$$\begin{aligned} v_{qd}^{\ell+1} = w^{\ell} v_{qd}^{\ell} + c_P^{\ell}\, \text{rand}_P\, (p_{\text{best},qd} - p_{qd}^{l}) \\ + c_G^{\ell}\, \text{rand}_G\, (g_{\text{best},d} - p_{qd}^{\ell}), \end{aligned} \tag{9}$$

where the 1st, 2nd, and 3rd terms correspond to the contributions from the old velocity of the particle, P_{best}, and G_{best} vectors, respectively; w^{ℓ} refers to the inertia weight, which controls the impact of old velocity on the new value; c_P^{ℓ} and c_G^{ℓ} denote the weights for controlling P_{best} and G_{best} contributions to the new velocity; and rand_P and rand_G are random numbers taking values between 0 and 1, respectively. Defining Δt as the time step (which is set to 1), the new position of the particle q at iteration $\ell + 1$ for variable d is given by:

$$p_{qd}^{\ell+1} = p_{qd}^{\ell} + v_{qd}^{\ell+1} \Delta t. \tag{10}$$

In our simulations we take $0.4 \leq w^{\ell} < 0.9$ as the appropriate interval allowing a good performance for the algorithm [12]. Also, the new positions of the particles that exceed the solution space boundaries are clipped to the boundaries.

B. UAV Location Tuning Using PSO

The flow chart of the proposed PSO-based UAV location optimization is depicted in Fig. 2. Firstly, random positions and velocities for each particle are generated prior to evaluation of their associated UAV locations in the ZF pre-coding. The considered optimization problem targets decreasing the correlation in $\boldsymbol{H}$ for maximization of the sum-rate, $\sum_{j=1}^{N_r} R_j$. To calculate the correlation in $\boldsymbol{H}$, the 2-norm condition number, denoted $\text{cond}(\boldsymbol{H})$, is considered, which is defined as the ratio of the largest singular value of $\boldsymbol{H}$ to the smallest one. To decrease this correlation, we consider minimizing $\text{cond}(\boldsymbol{H})$.

The variables used for controlling $\text{cond}(\boldsymbol{H})$ are the UAVs' locations that directly impact $\boldsymbol{H}$, and are optimized using PSO. The sum-rate and $\text{cond}(\boldsymbol{H})$ for the corresponding network configuration are used to determine a fitness function F for evaluating the solution quality. Here, we consider:

$$F = F_1 \times \sum_{j=1}^{N_r} R_j - F_2 \times \text{cond}(\boldsymbol{H}) - (F_3 \times N_0), \tag{11}$$

where N_0 is the number of users with no LOS link with any AP. The 1st term in (11) promotes the solutions with higher sum-rates, the 2nd term downgrades those resulting in a poor condition number of $\boldsymbol{H}$, and the 3rd term avoids solutions with users experiencing blocked LOS. Constants F_1, F_2, and F_3 control the contribution of the different terms. Note that, minimizing $\text{cond}(\boldsymbol{H})$ may result in a less optimal sum-rate performance compared with when maximizing the sum-rate directly. However, the former approach results in a lower probability of obtaining an ill-conditioned $\boldsymbol{H}$. Based on the value of F, both P_{best} and G_{best} are updated, followed by calculating the new position and velocity of the particle in the solution space. After evaluating each particle for all iterations, the G_{best} vector will contain the optimized UAV locations.

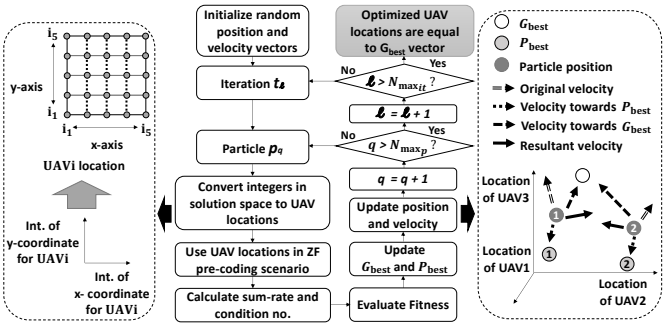

Fig. 2: Flow chart of the proposed algorithm for location optimization of three UAVs, where ℓ and q are the indexes of the number of iterations and particles, respectively. Dashed boxes on the left and right illustrate how UAV locations are converted to integers (Int.), and how two particles move in the solution space to find the optimal solution, respectively.

To manage how particles search for the optimal solution in the solution space and benefit from their experiences, the weight c_P^l in (9) is decreased from 2.5 (at the start of optimization) to 0.5 (at the end) for a better exploration of the solution space at the beginning by maximizing the reliance on P_{best}. On the other hand, for G_{best}, c_G^l is increased from 0.5 (at the start of optimization) to 2.5 (at the end) to enhance the convergence to the optimal solution [12].

The complexity of the proposed optimization mainly depends on calculating the particles' locations in PSO, evaluating the fitness function, and ZF pre-coding. For the considered PSO algorithm, the time and space complexities are $O(N_{\max_{it}} \times N_{\max_p} \times D)$ and $O(N_{\max_p} \times D)$, respectively [12].

IV. Performance Analysis

For the two cases of indoor industrial and outdoor scenarios, consider 4 LED-based APs, each mounted on a rotary-wing UAV, and 4 Rxs positioned at a height of 0.85 m above the floor level. The key system parameters are given in Table I. Considering a 10 MHz system bandwidth, the sum-rate R_j corresponding to the 1st term in (11) will be around tens of Mbps, whereas $\text{cond}(\boldsymbol{H})$ can reach orders of 10^3. Therefore,

TABLE I: Simulation parameters

Parameter	Value
LED conversion efficiency $\mathcal{S}$	0.44 W/A [9]
Transmit power per LED	15.84 W
LED Lambertian order m	1
Noise power spectral density (indoor/outdoor night)	10^{-21} A^2/Hz [10]
Link bandwidth	10 MHz [10]
PD responsivity ρ_j	0.4 A/W [10]
PD area	1 cm^2 [10]
Optical Rx FOV	62 deg. [8]
Rx height	0.85 m [8]

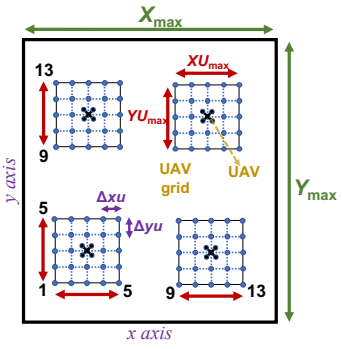

Parameter	Indoor (m)	Outdoor (m)
X_{max}	10	20
Y_{max}	10	20
XU_{max}	2	4
YU_{max}	2	4
Δxu	0.5	1
Δyu	0.5	1
UAV height	8	12

Fig. 3: Top view for the grid of possible UAV locations and the parameters considered for indoor industrial and outdoor scenarios.

we set F_1, F_2, and F_3 to 1, 10^5, and 10^{10}, respectively, to prioritize LOS blockage avoidance, while degrading the solutions with large condition numbers. In fact, although for the considered UAV heights it is unlikely that a Rx experiences a LOS blockage, the 3$^{\text{rd}}$ term in (11) guarantees the applicability of the proposed algorithm to a wide range of scenarios. Figure 3 shows the top view for the considered communication environment, highlighting the grid of possible locations for the four UAVs, and the corresponding parameters for the considered indoor industrial and outdoor scenarios.

A. Effect of Parameter Optimization

To find the best combinations of the numbers of particles and iterations for a given number of evaluations, we compare in Fig. 4 the average sum-rate for different combinations of $N_{\max_p}$ and $N_{\max_{it}}$, over 1000 random user positions, for both indoor and outdoor scenarios. As shown, the average sum-rate improves with increasing $N_{\max_p} \times N_{\max_{it}}$. For the same evaluation number, generally, a higher average sum-rate is achieved for $N_{\max_p} > N_{\max_{it}}$, which is because of a better exploration of the solution space prior to converging to the optimal solution. Note that, lower sum-rates are achieved for the outdoor scenario since UAVs are considered with higher altitudes with the same transmit power as for the indoor case. Also, note that the required number of evaluations is much smaller than when evaluating all possible solutions (4 UAVs,

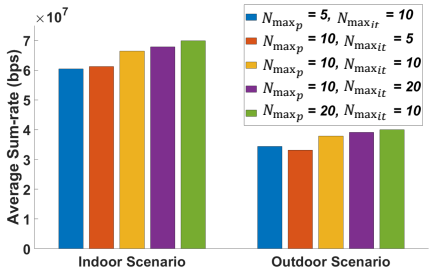

Fig. 4: Effect of $N_{\max_p}$ and $N_{\max_{it}}$ on the average sum-rate of 4 Rxs with 1000 random positions, in indoor industrial and outdoor scenarios.

with 25 possible locations each, see Fig. 3). Based on these results, we set $N_{\max_p} = 20$ and $N_{\max_{it}} = 10$ in the sequel.

B. Case Study of UAVs With Optimized Locations

To see how the sum-rate improves with the proposed optimization through iterations, we consider in Fig. 5 an indoor industrial scenario with (x, y) of the Rxs' positions of (0.26, 4.63), (2.93, 3.55), (6.17, 3.18), and (7.54, 9.87). The evolution of the fitness function F, from (11), is illustrated in the dashed blue boxes, together with the UAVs' location indexes (with respect to the grid), sum-rate, and cond($\boldsymbol{H}$), over every change in F (i.e., the best performance achieved). The dashed red box shows the case UAVs are positioned at the center of their corresponding grid space. Also, at the right side, we have shown the optimal positions of the UAVs with respect to the Rxs positions. We notice that PSO converges at iteration 5 to the optimal solution. Meanwhile, no improvement is achieved from iteration 2 to 3, i.e., the new positions found in iteration 3 did not result in an improvement of G_{best}. In fact, in the first iterations, PSO focuses on the solution space exploration, rather than convergence to the optimal solution. It is worth mentioning that the obtained solution via PSO after convergence (i.e., a sum rate of 0.973×10^8 bps) is quite close to the global optimal solution of 1.007×10^8 bps, obtained via parameter sweep (with considerably higher complexity).

C. Optimizing UAV Locations in Case of Mobility

In a dynamic scenario where the Rxs move around, the UAVs' locations need to be updated accordingly to ensure the best network performance. Figure 6 shows a comparison of the average sum-rate over different Rx mobilities, for the indoor industrial and outdoor scenarios, for different optimization rates used. For each mobility case, 1000 users' positions are generated according to the random way-point mobility model, where the time interval between each two successive positions is set to 0.5 sec. The considered maximum user speeds of 0.5 and 1.4 m/s correspond to walking and fast walking users, whereas the cases of 2 and 5 m/s correspond to equipment movements in current and future industrial scenarios [15], respectively. The considered time interval between optimizations are 0.5, 1, 2, and 5 sec. We have also considered the non-optimized cases where UAVs are located at their grid space in order to vary the inter-UAV distances from the minimum to the maximum. For the case of indoor scenario, as UAVs get closer, the similarity in the users' channel gains increases, resulting in

This article has been accepted for publication in a future issue of this journal, but has not been fully edited. Content may change prior to final publication. Citation information: DOI 10.1109/LWC.2021.3119221, IEEE Wireless Communications Letters

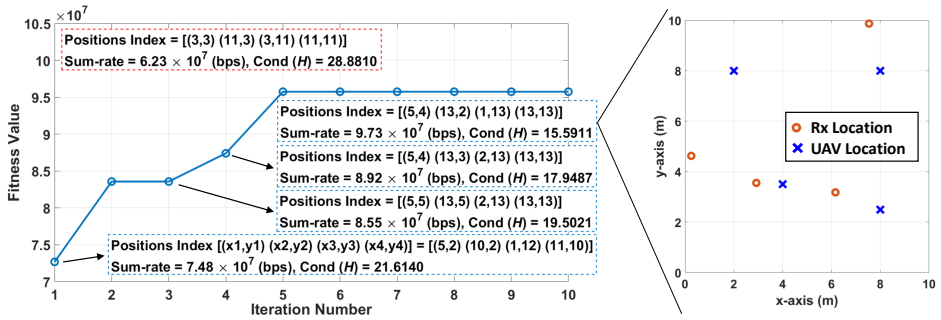

Fig. 5: Evolution of fitness value over iterations. Blue and red boxes correspond to optimized and non-optimized cases, respectively.

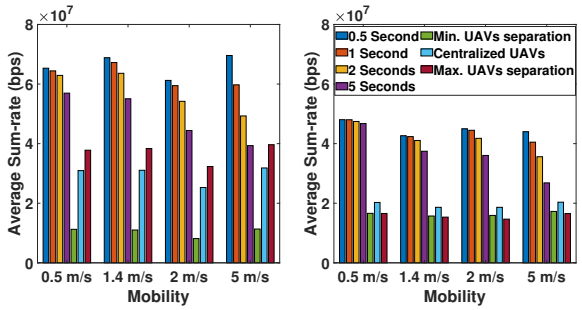

(a) (b)

Fig. 6: Comparison between optimized and non-optimized UAV locations for different user mobilities for (a) indoor industrial and (b) outdoor scenarios, considering different optimization update intervals.

an increased correlation in $\boldsymbol{H}$, and subsequently a decreased sum-rate. For outdoor scenarios, the advantages of maximizing the inter-UAV distances are reduced due to the increased path loss (due to increased LOS path length between the UAVs and the Rxs). Given the highlighted trade-off between the decrease in the channel correlation and the increase in the channel gain, the maximum distance between UAVs should be constrained in the system design by parameters such as the users' data rate requirements. On the other hand, results show an improved performance for optimized UAVs' locations for all cases. As expected, decreasing the optimization rate results in a performance degradation, which is more considerable with increased mobility. Indeed, larger variations in the users' positions over the given time window results in a faster deviation from the optimal UAVs configuration. Interestingly, even for the highest mobility case, updating optimized UAV positions at the lowest rate (i.e., every 5 sec) offers an improved performance, thus demonstrating the robustness of the proposed optimization.

V. Conclusions

We proposed optimization of the UAV locations using PSO, for MU-MISO ZF pre-coded UAV-based VLC networks and demonstrated the achieved performance improvement. We showed the importance of carefully choosing the fitness function as well as the adequate number of particles for a sufficient exploration of the solution space. Generally, as the number of variables (i.e., UAVs) increases, a larger number of evaluations should be considered to avoid being trapped in local solutions. We also considered different mobility scenarios and showed the robustness of the proposed solution for different optimization rates due to limited computational resources and/or high user mobility. The proposed optimization could be extended to carry out the pre-coder design while accounting for CSI uncertainty due to outdated or noisy CSI, as proposed in [9], which could be addressed in a future work.

References

[1] Z. Ghassemlooy, L. N. Alves, S. Zvanovec, and M. A. Khalighi, Eds., *Visible Light Communications: Theory and Applications*. CRC-Press, 2017.

[2] H. Deng, J. Li, A. Sayegh, S. Birolini, and S. Andreani, "Twinkle: A flying lighting companion for urban safety," in *Int. Conf. Tangible, Embedded, and Embodied Interaction*, Mar. 2018, Stockholm, Sweden.

[3] Y. Yang, M. Chen, C. Guo, C. Feng, and W. Saad, "Power efficient visible light communication with unmanned aerial vehicles," *IEEE Commun. Lett.*, vol. 23, no. 7, pp. 1272–1275, 2019.

[4] Y. Wang, M. Chen, Z. Yang, T. Luo, and W. Saad, "Deep learning for optimal deployment of UAVs with visible light communications," *IEEE Trans. Wireless Commun.*, vol. 19, no. 11, pp. 7049–7063, 2020.

[5] Q. V. Pham, T. Huynh-The, M. Alazab, J. Zhao, and W. J. Hwang, "Sum-rate maximization for UAV-assisted visible light communications using NOMA: Swarm intelligence meets machine learning," *IEEE Internet of Things J.*, vol. 7, no. 10, pp. 10 375–10 387, 2020.

[6] M. W. Eltokhey, M. A. Khalighi, and Z. Ghassemlooy, "Multiple access techniques for large space indoor scenarios: A comparative study,," in *Int. Conf. Telecommunications (ConTEL)*, July 2019, Graz, Austria.

[7] D. Gesbert, M. Shafi, D.-s. Shiu, P. J. Smith, and A. Naguib, "From theory to practice: an overview of MIMO space-time coded wireless systems," *IEEE J. Sel. Areas Commun.*, vol. 21, no. 3, pp. 281–302, 2003.

[8] Z. Yu, R. J. Baxley, and G. T. Zhou, "Multi-user MISO broadcasting for indoor visible light communication," in *Int. Conf. Acoustics, Speech Sig. Proc. (ICASSP)*, May 2013, pp. 4849–4853, Vancouver, Canada.

[9] H. Ma, L. Lampe, and S. Hranilovic, "Coordinated broadcasting for multiuser indoor visible light communication systems," *IEEE Trans. Commun.*, vol. 63, no. 9, pp. 3313–3324, Sept. 2015.

[10] M. W. Eltokhey, M. A. Khalighi, A. S. Ghazy, and S. Hranilovic, "Hybrid NOMA and ZF pre-coding transmission for multi-cell VLC networks," *IEEE Open J. Com. Soc.*, vol. 1, pp. 513–526, 2020.

[11] T. V. Pham, H. L. Minh, and A. T. Pham, "Multi-cell VLC: Multi-user downlink capacity with coordinated precoding," in *Int. Conf. Commun.*, May 2017, pp. 469–474, Paris, France.

[12] M. W. Eltokhey, K. R. Mahmoud, Z. Ghassemlooy, and S. S. Obayya, "Optimization of intensities and locations of diffuse spots in indoor optical wireless communications," *Opt. Switching Net.*, vol. 33, pp. 177–183, 2019.

[13] M. S. Demir, S. M. Sait, and M. Uysal, "Unified resource allocation and mobility management technique using particle swarm optimization for VLC networks," *IEEE Ph. J.*, vol. 10, no. 6, pp. 1–9, 2018.

[14] J. Kennedy and R. Eberhart, "Particle swarm optimization," in *Int. Conf. Neural Net.*, vol. 4, Nov. 1995, pp. 1942–1948 vol.4, Perth, Australia.

[15] C. Sauer, M. Schmidt, and M. Sliskovic, "Delay tolerant networks in industrial applications," in *Int. Conf. Emerging Technol. Factory Automation (ETFA)*, Sep. 2019, pp. 176–183, Zaragoza, Spain.